Micromechanics of a carbon nanotube turf and numerical modeling of nanoindentation

H. Radhakrishnan[1], S.Dj. Mesarovic[1,a], C.M. McCarter[1], D.F. Bahr[1], C.D. Richards[1]

School of Mechanical and Materials Engineering, Washington State University, Pullman WA 99163, USA

[a] mesarovic@mme.wsu.edu

Keywords: Carbon nanotubes; Nanoindentation; Micromechanical model; Finite element method; Adhesive contact.

Abstract. Carbon nanotubes grown on a substrate form a *turf* – a complex structure of intertwined, mostly nominally vertical tubes, cross-linked by adhesive contact and few bracing tubes. The turfs are compliant and good thermal and electrical conductors. In this paper, we consider the micromechanical model of the turf [Mesarovic et al, 2007, *Scripta Mat* **56**, 157-60], and develop a finite element implementation to simulate nanoindentation tests on CNT turfs. The model includes: nonlinear elastic deformation, small Kelvin-Voigt type relaxation, caused by the thermally activated sliding of contacts, and, adhesive contact between the turf and the indenter. The pre-existing (locked-in) strain energy of bent nanotubes produces a high initial tangent modulus, followed by an order of magnitude decrease in the tangent modulus with increasing deformation. The strong adhesion between the turf and indenter tip is due to the van der Waals interactions. The finite element simulations represent the results from the nanoindentation experiments with remarkable accuracy, including the loading, visco-elastic relaxation, unloading and adhesive pull-off.

Introduction

Since their discovery in the early nineties [1], the superior mechanical [2], electrical [3] and thermal [4] properties of carbon nanotubes (CNTs) have been extensively studied. While the earlier studies focused of the properties of individual carbon nanotubes, some recent studies addressed the mechanical behavior of simple assemblies: short widely spaced tubes [6, 7] and the lateral loading of parallel tubes in full contact [8].

Of interest here is the mechanical behavior of CNT turf (Fig. 1) – a complex network of intertwined CNTs. The turf is compliant and expected to be ideal candidate for use in a MEMS thermal switch [5]. In an earlier communication [9], we have analyzed in detail the mechanism of deformation of the turf under moderate strains by means of: (a) analysis of experimental results – standard and continuous indentation, and, (b) micromechanical scaling analysis. In this paper we develop a finite element model of the nanotube turf capable of reproducing the results from nanoindentation experiments. The turf is modeled as a nonlinear elastic continuum with the appropriate time-dependent response. A phenomenological contact law is implemented to simulate the adhesion between the turf and the indenter.

The paper is organized as follows. First, we briefly describe the structure of the turf, experimental observations, and the micromechanical model [9]. We then describe the finite element formulation, present computational results and compare them to the experimental data.

Structure and micromechanics of a CNT turf

As shown in Fig. 1, most nanotubes in the turf are nominally vertical and slightly curved, while some segments are inclined or even horizontal. The contacts between adjacent tubes are van der

Waals bonded [10]. CNTs have high surface energy in air and low interface energy, so the system tends to lower its energy through contact. Thus, the total energy of the assembly, E, is given as

$$E = U - \Gamma , \tag{1}$$

where U is the total elastic bending energy of CNTs, while Γ is the contact (adhesive) energy, defined as the difference between the total interface and surface energy of the assembly and the surface energy of an imaginary contact-free assembly. As the configurational space is very large, many energy minima are expected. However, the experimentally observed mechanical reversibility [5, 9] indicates broad convex regions around the minima, so that – after moderate strains – the structure returns to its initial state. Nominally, the absolute energy minimum is achieved when the structure collapses laterally, i.e., with all tubes straight and in full contact. During initial stages of growth, the collapse is prevented by the substrate constraint. As the turf grows, the inclined and horizontal segments prevent the lateral collapse. We note that the turf is indeed a *material*; it retains its structural integrity after the removal of the substrate [12].

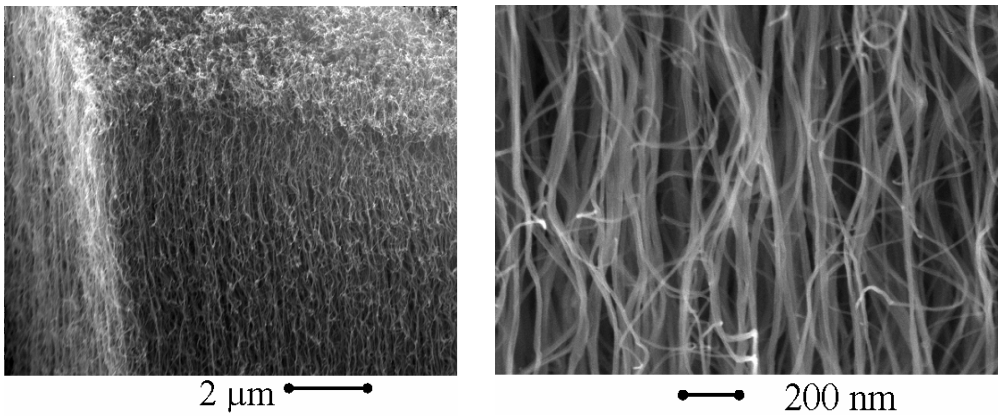

Fig. 1. SEM images of the carbon nanotube turf.

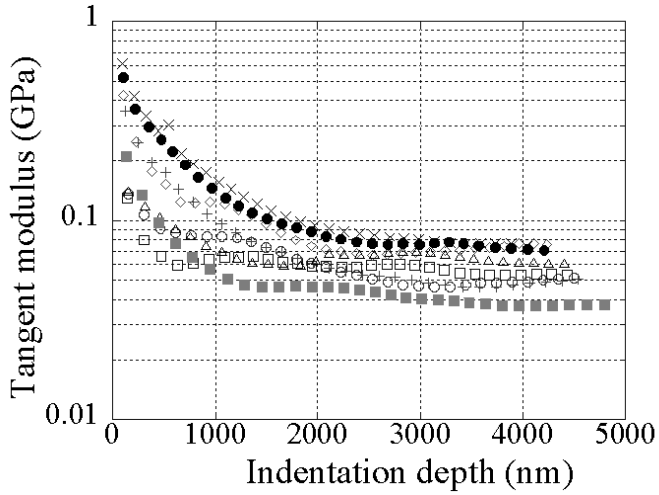

Fig. 2. Results from continuous stiffness indentation experiments. The test is carried by small oscillations with the time period small compared to the characteristic relaxation time of the turf, so that the viscous relaxation is negligible. The more compliant cases are from the indentations closer to the edge of the turf.

The standard nanoindentation experiments (Hysitron Triboscope with a broad Berkovich tip) were carried on CNT turfs [5, 9], with the following conclusions (cf. Fig. 7): (a) for moderately large strains the deformation is fully reversible, (b) the turf exhibits time dependent relaxation, (c) the load – indentation depth curve for the initial spherical portion of the indentation is linear, and, (d) during the retraction phase the indenter experiences strong adhesion with the turf.

The mechanism of deformation in the turf is easily understood by means of a simple micromechanical model of a free CNT segment with an initial curvature and contact patches at both the ends [9]. Extended to the behavior of an assembly of such segments, the model implies a high

initial tangent modulus followed by a rapid decrease in tangent modulus with increasing strain. This has been tested in the continuous stiffness indentation tests [11]. The results shown in Fig. 2 [9] are consistent with the micromechanical model developed; the turf exhibits a high initial tangent modulus followed by an order of magnitude decrease in its value at moderate strains. During the loading portion of the indentation, such material behavior yields results similar to those obtained by indenting an elastic – ideally plastic solid [13]. Hence the linear force displacement curve (Fig. 7) mentioned before. At larger strains deformation ceases to be reversible [10, 20].

The mechanism of viscous relaxation is the thermally activated sliding and rearrangements of inter-CNT contacts.

Finite element model

The finite element (FE) model of the turf is developed by treating the turf as a continuum. Modeling of the actual nanostructure would require discretization of each CNT into segments with an appropriate model the interaction between the segments, thus making the analysis computationally expensive.

Given its structure, the CNT turf is expected to be orthotropic in the plane orthogonal to the direction of growth of the nanotubes. However, the experiments on nanoscale are limited by the difficulties of manipulating the sample, so that the number of independent materials constants obtained experimentally is limited, too. Therefore, we use a simple isotropic model.

The complete FE model requires the use of an appropriate nonlinear elastic model with a response similar to that seen in the continuous stiffness measurements (Fig. 2), combined with the time dependent relaxation. Further, the model also requires the implementation of a contact law to simulate the strong adhesion between the turf and the indenter. We use the commercial finite element software ABAQUS [14] and its user-defined subroutine features to model the contact law.

The material model. The Green hyper-elastic model [15] is commonly used for highly compressible materials. The strain energy density is expressed in terms of non-integer powers of principal stretches. This enables better fit to experimental data than other models with integer powers, such as the Mooney-Rivlin model.

To model the highly compressible CNT turf, we assume the zero Poisson's ratio. From the continuous indentation experiments (Fig. 2), the ratio of the initial tangent modulus to that at moderate strains is almost constant (≈ 10). The resulting uniaxial compression curve fit from the hyper-elastic material is shown in Fig. 3. The initial tangent modulus is 700 MPa, and decays to 70 MPa at moderate strains. The transition is controlled by the value of the non-integer power of the principal stretches with larger values implying a more rapid transition.

The time dependent relaxation is incorporated by assuming that the instantaneous shear modulus of the material $\mu(t)$, varies according to the relation

$$\mu(t) = \mu_0 e^{-t/\tau} + \mu_\infty \left(1 - e^{-t/\tau}\right), \tag{2}$$

where μ_0 is the initial shear modulus, τ is the characteristic relaxation time, and μ_∞ is the relaxed shear modulus. From the standard nanoindentation experiments, the characteristic relaxation time of the nanotube turf is estimated to be around 3 seconds [9].

The contact law. The adhesive contact between the diamond Berkovich tip and the CNT turf is due to the van der Waals interactions. The interaction between CNT walls is usually modeled using the Lennard-Jones type force law [16]:

$$p(\alpha) = (9\gamma/2\alpha_0)\left[(\alpha_0/\alpha)^{10} - (\alpha_0/\alpha)^4\right], \tag{3}$$

where p is the contact pressure, γ is the surface energy, and α_0 is the equilibrium inter-atomic spacing (0.34 nm). However the contact law (3) was intended for interaction between static CNT walls and cannot be directly used for the turf. The turf has free standing CNTs at the surface, which oscillate about their mean positions, resulting in the increased effective range of interactions. TEM observations [17] of the vibration amplitude of CNTs as function of temperature confirm their thermal origin. The root mean square of the vibration amplitude of a CNT supported at one end was computed as [17]

$$u^2 \approx 0.4243 kTl^3 \Big/ Y\left(r_0^4 - r_i^4\right), \tag{4}$$

where l is the free standing length (7 μm), k is the Boltzmann constant, T is the absolute temperature (300 K), Y is the elastic modulus of the nanotube (0.4 TPa), while r_0 and r_i are the outer (20 nm) and inner radii (17.3 nm) of the nanotube, respectively.

Using (4), the displacement of a typical CNT at the surface of the turf is computed as 4.64 nm and this value is taken to represent the range of interactions, α_{int} (Fig. 4). The value α_{int} is derived as the x-intercept of the tangent to the zero curvature point in (3). The modified force law (3) is flattened with a reduced maximum tensile traction but with the same surface energy as the original curve (Fig. 4).

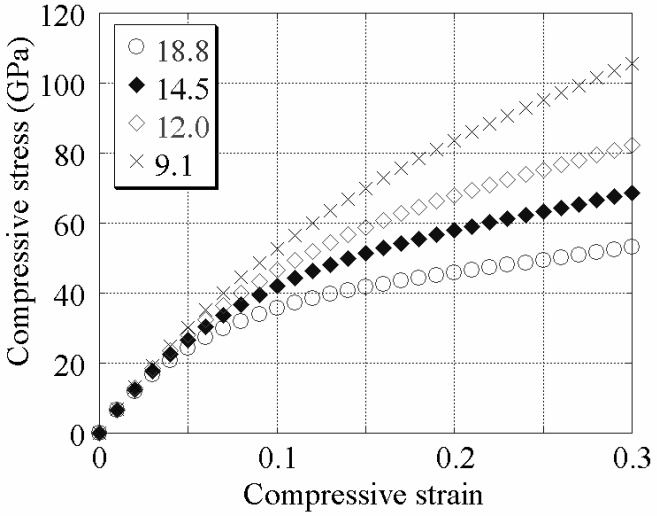

Fig. 3. Uniaxial compressive stress-strain curve using the Green hyper-elastic material model for different values of non-integer powers of principal stretches.

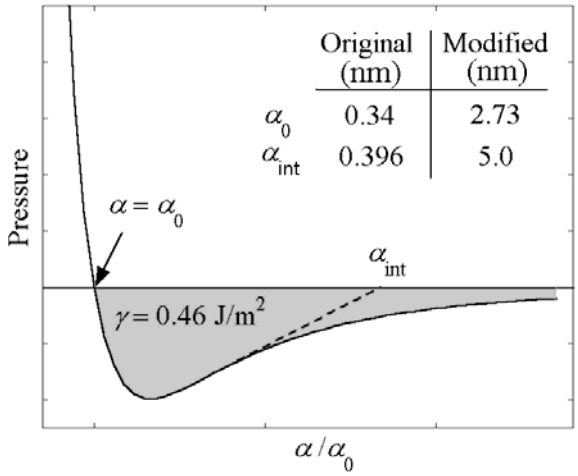

Fig. 4. Contact law used to model the van der Waals forces between the turf and the indenter. The original curve (3) is modified to include the effects of thermal vibration of the ends of the nanotube.

Results and Discussion

The FE analysis of the spherical (rotationally symmetric) nanoindentation was performed using both linear and quadratic 2D elements. During the initial approach of the indenter, an unstable jump-to-contact occurs (Fig. 5), as expected [18]. The numerical for such unstable jump include arc-length algorithm and dynamic formulation with an artificial viscous damping. These were thoroughly tested and are described in [19]; here, we only illustrate the behavior. In Fig. 5, the slope of the load-depth curve depends on the stiffness of the indentation mechanism (inset).

We begin with a simple loading mechanism (Fig. 5, inset) and a simple loading mechanism (Fig. 6, inset) to calibrate the power in the Green hyper-elastic model (Fig. 6) to the spherical loading portion of the indentation test (cf. Fig. 7a).

The actual loading mechanism of the Hysitron Triboscope is described in [9] and its schematic is illustrated in Fig. 7a (inset). The actual loading history is shown in Fig. 7b.

Computational and experimental results are compared in Fig. 7. It is evident that computational results fit the experiments remarkably well. In particular, the spherical loading portion (h<70 nm), relaxation (the top of the curve) and the pull-off load are fitted perfectly. The pyramidal portion of the Berkovich indenter (h>70nm) cannot be modeled with 2D rotationally symmetric setup.

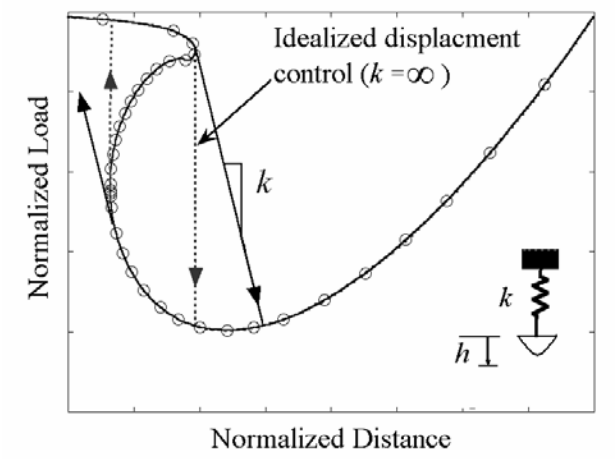

Fig. 5. Indentation of elastic solids with the loading mechanism shown in the inset. The open circles are the computational results using the arc-length algorithm.

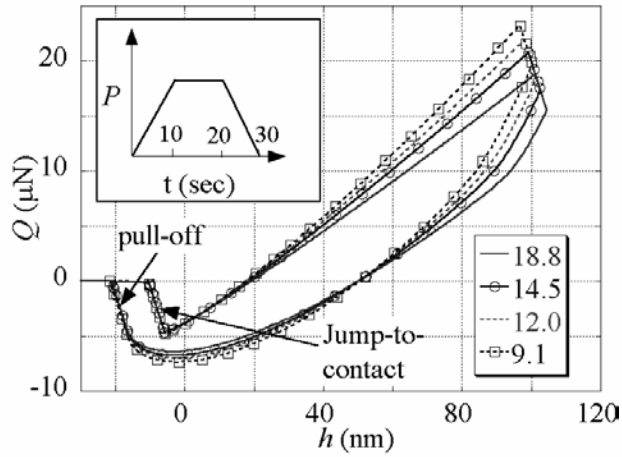

Fig. 6. True load-depth curves for different values of non-integer power. $\tau = 3$ sec, $\mu_\infty / \mu_0 = 0.6$. Inset: Loading profile.

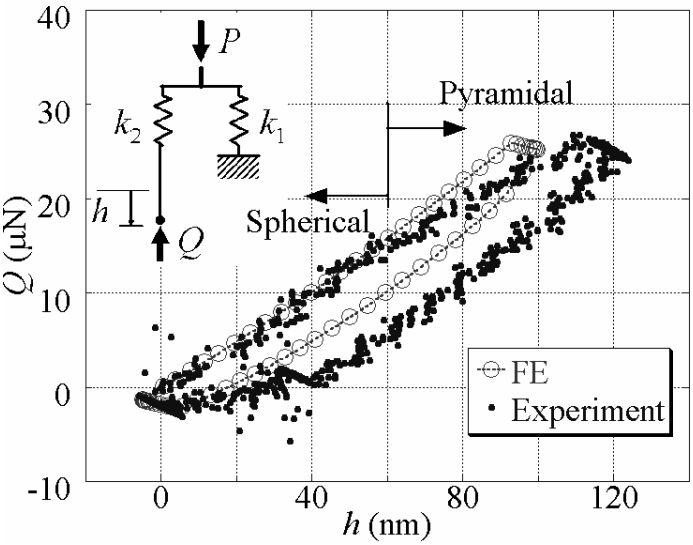

a)

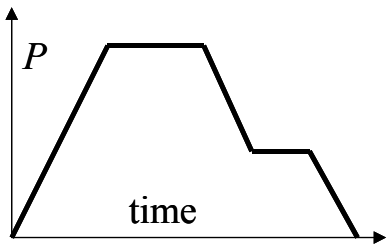

b)

Fig. 7. (a) Comparison between FE and nanoindentation experimental results. Inset: The loading mechanism of the Hysotron Triboscope used in the FE model. (b) Loading history.

Acknowledgements

This work has been supported in part by the US National Science Foundation, grant # CTS-0404370. The authors are grateful to J. Jiao and D. McClain, Portland State University, for providing the initial turf samples.

References

[1] Ijima, S. Nature. 354 (1992), p. 56-58.

[2] Bernholtz, J., Brenner, D., Buongiorno Nardelli, M., Meunier, V., Roland, C. Annu. Rev. Mater. Res. 32 (2002), p. 347.

[3] Kim, P., Shi, L., Majumdar, A., McEuen, P.L. Phys. Rev. Lett. 87 (21) (2001), p. 215502.

[4] Osman, M.A. and Srivastava, D. Nanotechnology 12 (2001), p. 21.

[5] McCarter, C.M., Richards, R.F, Mesarovic, S.Dj, Richards, C.D., Bahr, D.F., McClain, D., Jiao, J. J. Mater. Sci. 41 (2006), p. 7872-7878.

[6] Qi, H.J., Teo, K.B.K., Lau, K.K.S., Boyce, W.I., Milne, W.I., Robertson, J., Gleason, K.K. J. Mech. Phys. Solids. 51 (2003), p. 2009.

[7] Waters, J.F., Riester, L., Jouzi, M., Guduru, P.R., Xu, J.M. Appl. Phys. Lett. 85 (10) (2004), p. 1787-1789.

[8] Liu, J.Z., Zheng, Q.S., Wang, J.F., Jiang, Q. J. Mech. Phys. Solids. 53 (2005), p. 123.

[9] Mesarovic, S.Dj., McCarter, C.M., Bahr, D.F., Radhakrishnan, H., Richards, R.F., Richards, C.D., McClain, D., Jiao, J. Scripta Mat. 56 (2007) p. 157-160.

[10] Ajayan, P.M., Banhart F. Nat. Mater. 3 (3) (2004) p.135.

[11] Oliver, W.C, Pharr, G.M. J. Mater. Res. 7 (6) (1992) p. 1564.

[12] Yurdumakan, B, Raravikar, N.R., Ajayan, P.M., Dhinojwala, A. Chem. Comm. (2005) p. 3799.

[13] Mesarovic S.Dj., Fleck N.A. Proc. R. Soc. Lond. A. 455 (1999), 2707-2728.

[14] ABAQUS 2004 V6.5 User's manual. Hibbitt, Karlsson & Sorensen Inc., Pawtucket, R.I.

[15] Storakers, B. J. Mech. Phys. Solids 34 (2) (1986) p. 125-145.

[16] Zhao, Y.X, Spain, I.L. Phys. Rev. B. 40 (2) (1989) p. 993-9970.

[17] Treacy, M.M.J., Ebbensen, T.W., Gibson, J.M. Nature 381 (1996) p. 678-680.

[18] Greenwood, J.A. Proc. R. Soc. Lond A. 453 (1997) p. 1277-1297.

[19] Radhakrishnan, H., Mesarovic, S. Dj. Submitted to J. Coll. Interf. Sci. (2007)

[20] Zbib, A.A., Mesarovic, S.Dj., Lilleodden, E., McClain, D., Jiao, J., Bahr, D. Submitted to Science (2007)